Slender piezoelectric beams with resistive-inductive electrodes – modeling and axial wave propagation

Juergen Schoeftner[*1], Gerda Buchberger[2a] and Ayech Benjeddou[3b]

[1]*Johannes Kepler University, Institute of Technical Mechanics, Altenbergerstrasse 69, 4040 Linz, Austria*
[2]*Johannes Kepler University, Institute of Biomedical Mechatronics, Altenbergerstrasse 69, 4040 Linz, Austria*
[3]*SUPMECA, 3 rue Fernand Hainaut, 93407 Saint Ouen CEDEX, France*

Abstract. This contribution presents an extended one-dimensional theory for piezoelectric beam-type structures with non-ideal electrodes. For these types of electrodes the equipotential area condition is not satisfied. The main motivation of our research is originated from passive vibration control: when an elastic structure is covered by several piezoelectric patches that are linked via resistances and inductances, vibrational energy is efficiently dissipated if the electric network is properly designed. Assuming infinitely small piezoelectric patches that are connected by an infinite number of electrical, in particular resistive and inductive elements, one obtains the Telegrapher's equation for the voltage across the piezoelectric transducer. Embedding this outcome into the framework of Bernoulli-Euler, the final equations are coupled to the wave equations for the longitudinal motion of a bar and to the partial differential equations for the lateral motion of the beam. We present results for the wave propagation of a longitudinal bar for several types of electrode properties. The frequency spectra are computed (phase angle, wave number, wave speed), which point out the effect of resistive and inductive electrodes on wave characteristics. Our results show that electrical damping due to the resistivity of the electrodes is different from internal (=strain velocity dependent) or external (=velocity dependent) mechanical damping. Finally, results are presented, when the structure is excited by a harmonic single force, yielding that resistive-inductive electrodes are suitable candidates for passive vibration control that might be of great interest for practical applications in the future.

Keywords: piezoelectric effect; conductive electrodes; linear elastic beam and bar modeling; vibration control; wave propagation

1. Introduction

Smart and intelligent structures are systems which are equipped with multi-functional materials. Candidates for active or passive multi-functional materials are piezoelectric materials. The piezoelectric effect characterizes the ability to transform a mechanical motion or deformation into an electrical signal (direct piezoelectric effect) or to cause deformations of a body due to electrical stimuli (converse piezoelectric effect). The first-mentioned effect is exploited in sensor

∗Corresponding author, Ph.D., E-mail: juergen.schoeftner@jku.at
[a] Ph.D. Student., E-mail: gerda.buchberger@jku.at
[b] Professor, E-mail: ayech.benjeddou@supmeca.fr

applications (e.g., structural health monitoring), whereas the latter one is used for actuation. Classical review works on this subject are Crawley (1994), Miu (1993) and Tzou (1998).

In general, the electrodes of the piezoelectric transducers are assumed to be perfectly conductive, i.e., the electrical potential over the electrode surface does not depend on the location. This contribution is concerned with the development of a theory for beam-type structures including the piezoelectric effect, but without assuming the equipotential area condition to be fulfilled over the electrodes. These are so-called lossy electrodes (=resistive or finitely conductive electrodes), where the electric potential depends on the location. The other type of electrodes, where the equipotential area condition is fulfilled, is denoted as ideal or perfectly conductive electrodes. Here, we are mainly interested in how far these electrodes, namely resistive-inductive electrodes, influence the motion of a slender beam-type structure. In particular how mechanical vibrations can be attenuated. A variation of the electric potential provides an additional degree of freedom which might lower the sensitivity and improve the robustness of piezoelectric devices for vibration control.

Forward (1979) is the first to use piezoelectric devices for passive vibration control. He damped vibrations of an optical system by attaching an electric network to the piezoelectric transducer. Almost all researchers, which apply piezoelectric devices on elastic host structures, either for actuation or sensing purposes, use piezoelectric transducers with ideal electrodes. For metal electrodes the assumption of a uniformly distributed electric potential over the electrodes is correct, but for polymer electrodes, the potential loss over the surface might not be neglected. Large area resistive electrodes have been successfully applied for position-sensitive touchpads, where the location of a pressure or heat source can be detected with the Telegrapher's equation, see Buchberger *et al.* (2008), (2008b), (2015). To the best knowledge of the authors, the only investigations where non-perfect (=moderately conductive) electrodes are combined with elastic and piezoelectric systems are the contributions by Lediaev (2010) and Buchberger and Schoeftner (2013). In Lediaev (2010) the influence of moderately and high resistive electrodes on the three-dimensional deformations of a cantilever is investigated. In Buchberger and Schoeftner (2013) the beam theory for piezoelectric laminates is combined with resistive electrodes. Based on these results, it was found that the local action of the piezoelectric transducers can be manipulated by the resistive electrode properties, and the concept of shape control was successfully applied and even experimentally verified, see Schoeftner *et al.* (2014), (2015) and the patent (Schoeftner and Buchberger 2013).

Nowadays piezoelectric transducers are commonly used to control mainly time-harmonic vibrations of beams and plates. For this topic the reader is referred to the literature analysis in Schoeftner *et al.* (2015b), which considers bending vibrations of a piezoelectric beam. Comparatively few papers dealt with piezoelectricity and waves, in particular extensional waves in bars. The books of Graff (1991), Kolsky (1963) and Rose (2004) provide a good theoretical overview on wave propagation in elastic solids. Jansson and Lundberg (2007) derived a three-port impedance model of a piezoelectric element that is attached to a bar. With this model the electrical (voltage, current) and the mechanical ports (force, velocity) are coupled by a 3×3 matrix with four independent entries. In a further contribution of Jansson and Lundberg (2008) this model was used for damping and controlling extensional waves. In Lin and Yuan (2001) PZT ceramic discs were mounted on an aluminum plate that generate and sense Lamb waves. A Mindlin plate theory model was adopted to consider the interaction between the actuators, the sensors and the host plate. The reflection and transmission of waves in a composite beam with a semi-infinite delamination was investigated in Yuan *et al.* (2008). The Timoshenko beam theory was used to study the portion

of transmitted and reflected power caused by an open (non-contact) or a closed (full contact) delamination. A hybrid approach for computing ultrasonic guided waves in an efficient manner was presented by Vivar-Perez *et al.* (2014). Their objective is to couple a higher-order finite element method (HO-FEM) for the piezoelectric actuators with analytical methods, which describe the host structure. With this procedure the numerical and computational effort can be reduced and also the difference of their results with ABAQUS-FE calculations was found negligible. Wave propagation in a periodic piezoelectric beam was investigated in Ding *et al.* (2013). The dynamic transfer matrix is derived from an energy formulation, which is needed to predict the propagation of waves along the piezoelectric beam. Krawczuk *et al.* (2006) presented four spectral elements derived from elementary and more refined bar theories, which are then compared. The dynamic transfer matrices were developed for the elementary, the Love, the Mindlin-Herrmann and the three-mode theory. For disturbance signals, which also excite higher modes, it was found that the Mindlin-Herrmann and the three-mode theory give accurate results.

In this contribution we treat piezoelectric slender beam-type structures that are covered by resistive-inductive electrodes: we consider the longitudinal and the lateral motion of the beam and we finally obtain three coupled partial differential equations for the axial and for the lateral deformation and also for the electric voltage across (or the electric potential of) the piezoelectric transducers. For many practical applications, these equations may be decoupled, thus the longitudinal and the lateral motion can be treated independently. We concentrate on the wave propagation in piezoelectric bars with non-ideal and ideal electrodes. The equations of motion for a piezoelectric bimorph are given in non-dimensional form and the influence of wave speeds, wave numbers and phase angles (=which are indicators for damping) as a function of the excitation frequencies are given for various electrode materials. In the end, the transient behavior of the wave front due to a time-harmonic impact load is given, which also demonstrates the damping capabilities of the electrode material.

2. Resistive-inductive electrodes - concepts

The mathematical model for the electrodes can be derived from the equivalent circuit diagram given in Fig. 1: the electrodes consist of infinitely small electrical impedances which link the infinitely small piezoelectric patches (=represented by electric potential nodes $\phi(x, y)$, Fig. 1(c)). The one-dimensional representation is given in Fig. 1(d): assuming no gap between the patches ($d \rightarrow 0$) and that the lengths of the patches approach zero ($\Delta x \rightarrow dx$), one derives a model for the piezoelectric transducer, where the potential over the electrodes ϕ is not uniformly distributed. This means that the resistance per unit length $r(x) \neq 0$ and the inductance per unit length $l(x) \neq 0$ cause a voltage drop.

The electrical model of the infinitely small piezoelectric strips and the finitely conductive electrodes can be modeled as a transmission line (see Buchberger *et al.* (2008) and section 3.2). Combining these properties with the mechanical assumptions for a slender beam (equivalent single layer theory, Bernoulli-Euler framework including axial deformation of the beam axis, see Buchberger and Schoeftner (2013) and section 3.1), one derives new sets of differential equations for a piezoelectric laminated bar or/and beam with non-ideal resistive-inductive electrodes.
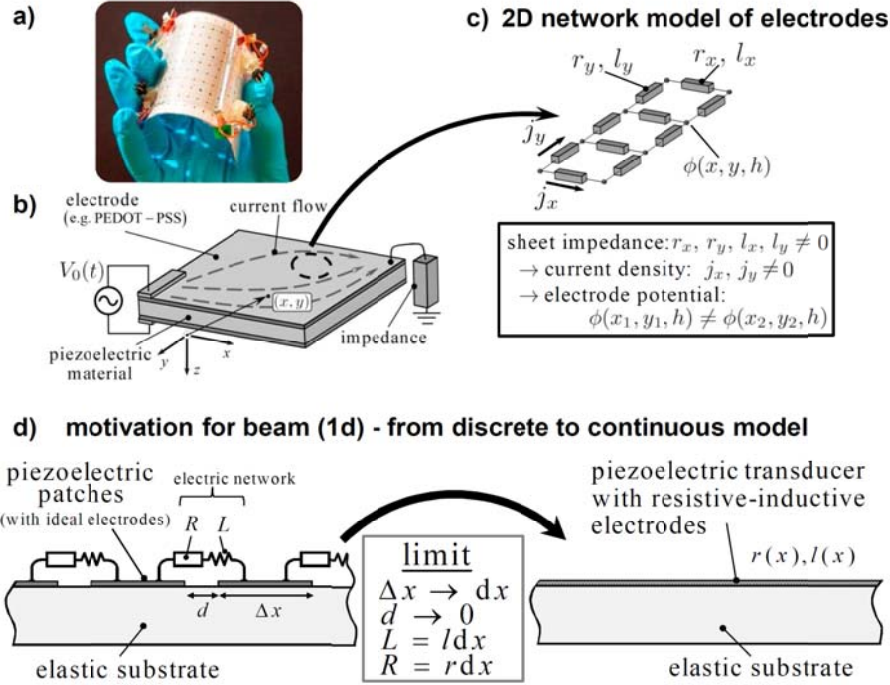
Fig. 1 (a) and (b) Prototype with electrodes of the conducting polymer poly(ethylene dioxythiophene) (PEDOT-PSS) (with friendly permission of Buchberger *et al.* (2008), (c) two-dimensional electrical model of the electrode surface, (d) one-dimensional discrete and continuous electrode model

3. Equations of motion of a slender piezoelectric beam with resistive-inductive electrodes

3.1 Electromechanical equations of piezoelectric beams

The displacements $u_0(x,t)$ and $w_0(x,t)$ of the x-axis and the axial strain $\varepsilon_{xx}(x,z,t)$ are related to the displacements $u(x,z,t)$ and $w(x,z,t)$ of an arbitrary point on the cross section as

$$u(x,z,t) = u_0(x,t) - zw_{0,x}(x,t) \tag{1}$$

$$w(x,z,t) = w_0(x,t) \tag{2}$$

$$\varepsilon_{xx}(x,z,t) = u_{0,x}(x,t) - zw_{0,xx}(x,t). \tag{3}$$

Here we only consider the thickness component of the electric field E_z^k and of the electric displacement D_z^k and neglect the components in the x-direction.

Neglecting the magnetic field, one finds the relation between the electric field and the electric potential ϕ^k from the Maxwell-Faraday equations

$$E_z^k = -\phi_{,z}^k \tag{4}$$

The voltage drop across the electrodes $V^k(x,t)$ over the beam length is defined by

$$V^k(x,t) = \phi^k(x, z_{2k}, t) - \phi^k(x, z_{1k}, t), \tag{5}$$

where the tracer k is the indicator for the kth piezoelectric layer. The distances to the x-axis are z_{2k} and z_{1k} so that the height of a layer is $h_k = z_{2k} - z_{1k}$.

The constitutive relations are the material laws which relate mechanical (=axial stress σ_{xx}^k and strain ε_{xx}) and electrical variables (=electric displacement D_z^k and electric field E_z^k)

$$\sigma_{xx}^k = \tilde{C}_{11}^k \varepsilon_{xx} - \tilde{e}_{31}^k E_z^k \tag{6}$$

$$D_z^k = \tilde{e}_{31}^k \varepsilon_{xx} + \tilde{\kappa}_{33}^k E_z^k. \tag{7}$$

The ˜–symbol means that these parameters are the material constants reduced on beam level (=the reduced short-circuit elastic stiffness $\tilde{C}_{11}^k$, the effective stress piezoelectric coupling constant $\tilde{e}_{31}^k$ and the effective blocked (=strain-free) permittivity $\tilde{\kappa}_{33}^k$).

Gauss' law of electrostatics applied on slender beams yields that $D_{z,z}^k = 0$ holds so that

$$D_z^k(x,t) = \text{const.} \rightarrow \frac{1}{h_k} \int_{z_{1k}}^{z_{2k}} D_z^k(x,t)\, \mathrm{d}z = \text{const.} \tag{8}$$

Inserting Eqs. (3)-(5) and (7) into Eq. (8) one finds for the electric displacement

$$D_z^k(x,t) = \tilde{e}_{31}^k \left(u_{0,x} - z_{\mathrm{m}k} w_{0,xx} \right) - \frac{\tilde{\kappa}_{33}^k}{h_k} V^k(x,t). \tag{9}$$

Solving Eq. (7) for the electric field and using Eq. (9), one finds

$$E_z^k(x,z,t) = -\frac{V^k(x,t)}{h_k} - \frac{\tilde{e}_{31}^k}{\tilde{\kappa}_{33}^k} \left(z_{\mathrm{m}k} - z \right) w_{0,xx}, \tag{10}$$

where $z_{\mathrm{m}k} = (z_{1k} + z_{2k})/2$ is the mean distance of the kth-layer to the x-axis. Finally, the equation of motion for the extensional and lateral deflections of a slender piezoelectric beam with the piecewise constant mass per unit length $M_w = M_u$ can be derived from d'Alembert's principle (see e.g., Krommer (2001))

$$M_u \ddot{u}_0(x,t) - M_{uw} \ddot{w}_{0,x}(x,t) - N_{,x} = q_x(x,t) \tag{11}$$

$$M_w \ddot{w}_0(x,t) + \left(M_{uw} \ddot{u}_0(x,t) \right)_{,x} - M_{,xx} = q_z(x,t). \tag{12}$$

where $q_x(x,t)$ and $q_z(x,t)$ are distributed forces in the x and z-directions. The normal force $N(x,t)$ and the bending moment $M(x,t)$ are computed by inserting Eq. (10) into Eq. (6) and integrating with respect to the cross-section of the beam (with the infinitesimal area $dA = b_k dz$)

$$N(x,t) = \sum_k \int_{z_{1k}}^{z_{2k}} \sigma_{xx}^k(x,z,t) b_k \, dz = K_N u_{0,x}(x,t) - K_{NM} w_{0,xx}(x,t) + \sum_k \tilde{e}_{31}^k b_k V^k(x,t) \tag{13}$$

$$M(x,t) = \sum_k \int_{z_{1k}}^{z_{2k}} \sigma_{xx}^k(x,z,t) b_k z \, dz = K_{NM} u_{0,x}(x,t) - K_M w_{0,xx}(x,t) + \sum_k \tilde{e}_{31}^k b_k z_{mk} V^k(x,t). \tag{14}$$

Here, the axial, the coupling and the bending stiffness are denoted by K_N, K_{NM} and K_M and the mass per unit length by $M_w = M_u$ (see Appendix A), respectively.

3.2 Electric equations of the resistive-inductive electrodes

The models of the piezoelectric transducer and for the electrodes are shown in Fig. 2. The thickness of the electrodes is infinitely small and perfect bonding between the layers is assumed. The electrodes are modeled as a transmission line with the series resistance r_i^k and inductance l_i^k per unit length. The time-derivative of the electric displacement, which is proportional to the electric current, can be split up into elastic and electric portions: one is the current generated by the deformation di_{elast}^k, the other one is the leakage current di_c^k through the blocked capacitance per unit length $c^k = \tilde{\kappa}_{33}^k b_k / h_k$. Using Eq. (9) one obtains the infinitesimal current flow between the electrodes

$$di_D^k(x,t) = \dot{D}_z^k(x,t) b_k \, dx = di_{elast}^k(x,t) + di_c^k(x,t). \tag{15}$$

Applying Kirchhoff's current rules for the leakage flow between the electrodes and the voltage rule for the electrode surface, four differential equations are obtained (see Fig. 2).

$$\begin{aligned}
i_{1,x}^k &= -i_{D,x}^k = -\tilde{e}_{31}^k(\dot{u}_{0,x} - z_{mk}\dot{w}_{0,xx})b_k + c^k \dot{V}^k \\
i_{2,x}^k &= -i_{D,x}^k = \tilde{e}_{31}^k(\dot{u}_{0,x} - z_{mk}\dot{w}_{0,xx})b_k + c^k \dot{V}^k \dots \text{Kirchhoff's current rule (KCR)}
\end{aligned} \tag{16}$$

$$\begin{aligned}
-\phi_{,x}^k(x,z_{1k}) &= i_1^k r_1^k + \frac{di_1^k}{dt} l_1^k \\
-\phi_{,x}^k(x,z_{2k}) &= i_2^k r_2^k + \frac{di_2^k}{dt} l_2^k \dots \text{Kirchhoff's voltage rule (KVR)}.
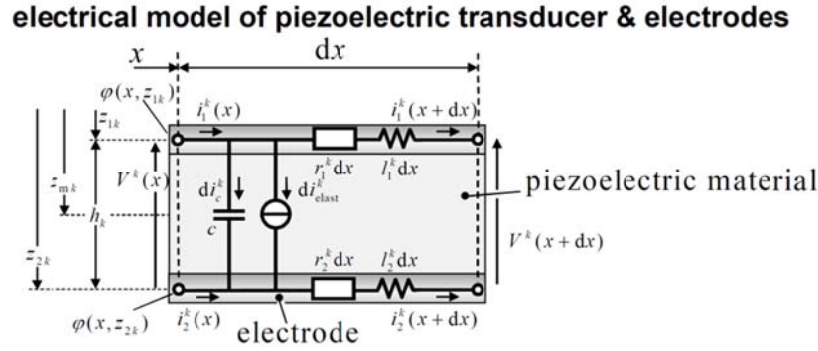\end{aligned} \tag{17}$$

electrical model of piezoelectric transducer & electrodes

Fig. 2 Model of a piezoelectric layer with resistive-inductive electrodes. The current flow between the layers $\mathrm{d}i_c^k, \mathrm{d}i_{\mathrm{elast}}^k$ influence the voltage difference $V^k(x,t)$ and consequently also the motions $u_0(x,t)$, $w_0(x,t)$ of the structure

Eq. (16) states the decrease/increase of the current over the electrodes is equal to the leakage current gradient $i_{D,x}^k$ between the electrodes. The first term on the right-hand side of Eq. (16) $\tilde{e}_{31}^k \left[\dot{u}_{0,x} - z_{\mathrm{m}k}\dot{w}_{0,xx} \right]b_k$ shows the coupling to the mechanical strain. The variation of the electric potential along the electrodes is given by Eq. (17), which is related to the electrode current i_i^k by the resistance r_i^k and the inductance l_i^k, i=1,2.

3.3 Coupled membrane-bending equations of motion

The $2+5k$ unknowns $u_0(x,t), w_0(x,t), V^k(x,t), \phi^k(x,z_{1k},t), \phi^k(x,z_{2k},t), i_1^k(x,t)$ and $i_2^k(x,t)$ of the partial differential equations can be solved by
   • The two equations of motion (11) and (12)
   • The k voltage-potential relations (5)
   • And the $4k$ Kirchhoff Eqs. (16) and (17).
   In order to focus on much more practical problems, we derive a less complex set of differential equations: we consider structures with constant properties along the x-coordinate, except for the electrode properties. Furthermore, we consider a bimorph consisting of two identical piezoelectric layers with the same direction of polarization, consequently, the coupling terms $K_{\mathrm{NM}}, M_{uw} = 0$ vanish. The resistance and inductance per unit length for the internal and external electrodes are identical $r_1(x) = r_2(x) = r(x), l_1(x) = l_2(x) = l(x)$ (Fig. 3). The potentials of the inner electrodes are grounded $\phi^1(x, z_{1\mathrm{l}} = z_{1\mathrm{p}}, t) = \phi^1(x, z_{2\mathrm{u}} = -z_{1\mathrm{p}}, t) = 0$.

Taking into account these simplifications and applying the Laplace transformation ($\mathcal{L}\{u_0(x,t)\} = \hat{u}_0(x,s), \mathcal{L}\{w_0(x,t)\} = \hat{w}_0(x,s), \mathcal{L}\{V^k(x,t)\} = \hat{V}^k(x,s)$), the following equations for the displacements $\hat{u}_0(x,s)$ and $\hat{w}_0(x,s)$ are derived from Eqs. (11)-(14)

$$M_u\hat{u}_0(x,s)s^2 - K_N\hat{u}_{0,xx}(x,s) = \hat{q}_x(x,s) + \tilde{e}_{31}^p b_p\left[\hat{V}_{,x}^1(x,s) + \hat{V}_{,x}^u(x,s)\right] \tag{18}$$

$$M_w\hat{w}_0(x,s)s^2 - K_M w_{0,xxxx}(x,s) = \hat{q}_z(x,s) + \tilde{e}_{31}^p z_{mp}b_p\left[\hat{V}_{,x}^1(x,s) - \hat{V}_{,x,x}^u(x,s)\right] \tag{19}$$

For the derivation of the electrical voltage equations for the lower and upper layers ($k = 1, u$), one differentiates Eq. (17) with respect to x, subtracts the second from the first equation, and then inserts Eqs. (5) and (16)

$$-\hat{V}_{,xx}^k(x,s) + \frac{[r(x)+sl(x)]_{,x}}{r(x)+sl(x)}V_{,x}^k(x,s) + cs[r(x)+sl(x)]\hat{V}^k(x,s)$$
$$= \tilde{e}_{31}^p b_p s[r(x)+sl(x)]\left[\hat{u}_{0,x}(x,s) - z_{mk}w_{0,xx}(x,s)\right] \text{ for } k = 1, u \tag{20}$$

The mechanical strain can be split into one part from the axial deflection $u_{0,x}$ and one part from the mean bending strain $z_{mp}w_{0,xx}(x,t)$: neglecting the bending strain, the voltage drop is identical for lower and upper layer $V(x,t) = V^1(x,t) = V^u(x,t)$. In contrast for $u_{0,x} = 0$, the bending strain $z_{mp}w_{0,xx}(x,t)$ causes sign-reversed voltages $V(x,t) = V^1(x,t) = -V^u(x,t)$, since it holds: $z_{m1} = z_{mp}$ and $z_{mu} = -z_{mp}$. The tedious transformation of Eqs. (18)-(20) into the time-domain is left out at this place.
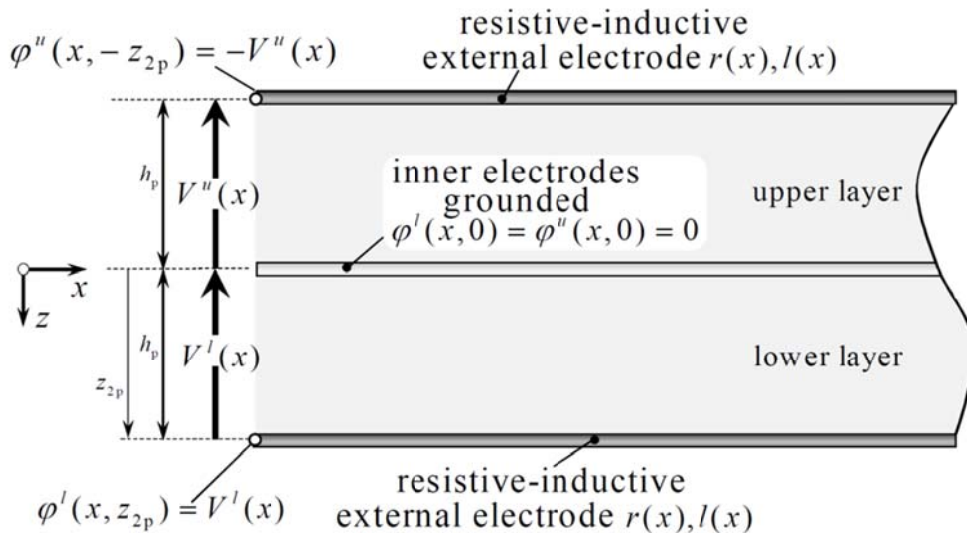

Fig. 3 Piezoelectric bimorph for which the differential Eqs. (18)-(20) are derived and which is used for the numerical example (section 4.3)

The main novelty of our modeling approach is given by Eq. (20), which determines the distribution of the voltage drop depending on the resistance and inductance per unit length of the electrode $r(x), l(x)$ and the axial strain $\hat{u}_{0,x}(x,s) - z_{\mathrm{m\,k}}\hat{w}_{0,xx}(x,s)$, the voltage $\hat{V}(x,s)$ may be computed. So this technology could be a promising candidate for passive vibration control, if the design of the inductive-resistive properties are well-tuned (see Fig. 8 and also Schoeftner *et al.* (2015b)).

4. Axial wave propagation analysis

4.1 Equations of motion of a slender piezoelectric bar

In the following we assume constant electrode properties $r_{,x}(x) = l_{,x}(x) = 0$ and additionally take into account internal D_{int} and external D_{ext} damping. Thus, setting $q_z = 0$, one finds the time-domain representation of Eqs. (18)- (20), yielding two coupled and damped wave equations

$$M_u \ddot{u}_0(x,t) + D_{\mathrm{ext}}\dot{u}_0(x,t) - D_{\mathrm{int}}\dot{u}_{0,xx}(x,t) - K_{\mathrm{N}}u_{0,xx}(x,t) = q_x(x,t) + 2\tilde{e}_{31}^{\mathrm{p}}b_{\mathrm{p}}V_{,x}(x,t) \tag{21}$$

$$-V_{,xx}(x,t) + cr\dot{V}(x,t) + cl\ddot{V}(x,t) = \tilde{e}_{31}^{\mathrm{p}}b_{\mathrm{p}}\left[r\dot{u}_{0,x}(x,t) + l\ddot{u}_{0,x}(x,t) \right] \tag{22}$$

In order to identify the problem-governing parameters, Eqs. (21) and (22) are transformed into non-dimensional differential equations. The speed of the axial wave is governed by $c_{\mathrm{mech}} = \sqrt{K_{\mathrm{N}}/M_u}$, the electrical wave by $c_{\mathrm{elec}} = \sqrt{1/cl}$. Introducing the characteristic length as L, the characteristic oscillations period as T and the characteristic voltage as $V_0 = K_{\mathrm{N}}/(\tilde{e}_{31}^{\mathrm{p}}b_{\mathrm{p}})$, one finds the non-dimensional coordinate, time, displacement and voltage as

$$\overline{x} = x/L \qquad \overline{t} = t/T \qquad \overline{u}_0 = u_0/L \qquad \overline{v} = V/V_0. \tag{23}$$

Consequently, one finds the non-dimensional coupled wave equations, with the non-dimensional load $\overline{q}_{\overline{x}} = q_x L/K_{\mathrm{N}}$, as

$$\tau_m \overline{u}_{0,\overline{t}\overline{t}} + d_{\mathrm{ext}}\overline{u}_{0,\overline{t}} - d_{\mathrm{int}}\overline{u}_{0,\overline{t}\overline{x}\overline{x}} - \overline{u}_{0,\overline{x}\overline{x}} = \overline{q}_{\overline{x}} + 2\overline{v}_{,\overline{x}} \tag{24}$$

$$-\overline{v}_{,\overline{x}\overline{x}} + \tau_r \overline{v}_{,\overline{t}} + \tau_l \overline{v}_{,\overline{t}\overline{t}} = \frac{\alpha^2}{2}\left[\tau_r \overline{u}_{0,\overline{t}\overline{x}} + \tau_l \overline{u}_{0,\overline{t}\overline{t}\overline{x}} \right]. \tag{25}$$

These equations show that the problem is governed by these six non-dimensional parameters only

$$\tau_m = \frac{L^2}{T^2 c_{\mathrm{mech}}^2} \qquad \tau_r = \frac{rcL^2}{T} \qquad d_{\mathrm{ext}} = \frac{D_{\mathrm{ext}}L^2}{TK_{\mathrm{N}}} \qquad d_{\mathrm{int}} = \frac{D_{\mathrm{int}}}{TK_{\mathrm{N}}} \qquad \tau_l = \frac{L^2}{T^2 c_{\mathrm{elec}}^2} \qquad \alpha^2 = \frac{2\tilde{e}_{31}^{\mathrm{p2}}b_{\mathrm{p}}^2}{K_{\mathrm{N}}c}. \tag{26}$$

4.2 Axial wave propagation solution under impact loads

For the numerical example presented in section 4.3.3, we need to determine the Green's functions of a bar that is subjected to the dirac-load $\overline{q}_{\overline{x}} = \delta(\overline{x})\delta(\overline{t})$. For this purpose, we apply the double-transform approach to our wave Eqs. (24) and (25), see Fig. 4 and also Graff (1991). First the Fourier transform is taken on the $\overline{x}$ -coordinate $\left[\overline{u}_0(\overline{x},\overline{t}),\overline{v}(\overline{x},\overline{t})\right] \rightarrow \left[\overline{U}(\overline{k},\overline{t}),\overline{V}(\overline{k},\overline{t})\right]$, and then the Laplace transform on the time $\left[\overline{U}(\overline{k},\overline{t}),\overline{V}(\overline{k},\overline{t})\right] \rightarrow \left[\overline{U}_{\mathrm{L}}(\overline{k},\overline{s}),\overline{V}_{\mathrm{L}}(\overline{k},\overline{s})\right]$ (Fig. 4). Assuming zero-initial conditions, it follows, from Eqs. (24) and (25), that

$$\begin{pmatrix} \tau_m \overline{s}^2 + \overline{k}^2 + d_{ext}\overline{s} + d_{int}\overline{k}^2\overline{s} & -2\overline{k}i \\ -\dfrac{\alpha^2}{2}(\tau_r\overline{s} + \tau_l\overline{s}^2)\overline{k}i & \overline{k}^2 + \tau_r\overline{s} + \tau_l\overline{s}^2 \end{pmatrix} \begin{pmatrix} \overline{U}_L \\ \overline{V}_L \end{pmatrix} = \begin{pmatrix} \overline{q}_{\overline{x}L} \\ 0 \end{pmatrix} \tag{27}$$

Inverting Eq. (27) yields the solution for the displacement and the voltage

$$\begin{pmatrix} \overline{U}_L \\ \overline{V}_L \end{pmatrix} = \frac{1}{\det} \begin{pmatrix} \overline{k}^2 + \tau_r\overline{s} + \tau_l\overline{s}^2 & 2\overline{k}i \\ \dfrac{\alpha^2}{2}(\tau_r\overline{s} + \tau_l\overline{s}^2)\overline{k}i & \tau_m\overline{s}^2 + \overline{k}^2 + d_{ext}\overline{s} + d_{int}\overline{k}^2\overline{s} \end{pmatrix} \begin{pmatrix} \overline{q}_{\overline{x}L} \\ 0 \end{pmatrix}$$

$$= \begin{pmatrix} G_{\overline{U}\overline{U}}(\overline{k},\overline{s}) & G_{\overline{U}\overline{V}}(\overline{k},\overline{s}) \\ G_{\overline{V}\overline{U}}(\overline{k},\overline{s}) & G_{\overline{V}\overline{V}}(\overline{k},\overline{s}) \end{pmatrix} \begin{pmatrix} \overline{q}_{\overline{x}L} \\ 0 \end{pmatrix} \tag{28}$$

where the determinant is the characteristic equation of the system

$$\det = \left(\tau_m\overline{s}^2 + \overline{k}^2 + d_{ext}\overline{s} + d_{int}\overline{k}^2\overline{s}\right)\left(\overline{k}^2 + \tau_r\overline{s} + \tau_l\overline{s}^2\right) + \alpha^2\left(\tau_r\overline{s} + \tau_l\overline{s}^2\right)\overline{k}^2. \tag{29}$$

The quantities $G_{\overline{U}\overline{U}}(\overline{k},\overline{s}), G_{\overline{U}\overline{V}}(\overline{k},\overline{s}), G_{\overline{V}\overline{U}}(\overline{k},\overline{s}), G_{\overline{V}\overline{V}}(\overline{k},\overline{s})$ are the transfer functions in the $(\overline{k}-\overline{s})$ -domain. For the numerical example presented in section 4.3.3, the external load is a time-harmonic impulse load $\overline{q}_{\overline{x}}(\overline{x},\overline{t}) = \delta(\overline{x})\cos(\overline{t})$. Knowing the Green's function $\overline{g}(\overline{x},\overline{t})$ of the displacement, which is the solution of the temporal and spatial impulse load $\overline{q}_{\overline{x}}(\overline{x},\overline{t}) = \delta(\overline{x})\delta(\overline{t})$, one may find more general load cases by the following double integral.

$$\overline{u}(\overline{x},\overline{t}) = \int\limits_{0}^{t}\int\limits_{-\infty}^{\infty} \overline{g}(\overline{x}-\overline{x}',\overline{t}-\overline{t}')\overline{q}_{\overline{x}}(\overline{x},\overline{t})\,\mathrm{d}\overline{t}'\,\mathrm{d}\overline{x}' \tag{30}$$

see e.g. Abramovich and Stegun (1972). In Graff (1991) pp. 25, it is shown how the Green's function is obtained for the wave equation. We extend here this solution procedure to the coupled wave Eqs. (24) and (25):

Performing the Fourier and Laplace transformation of the impulse load, it follows that $\overline{q}_{\overline{x}\mathrm{L}}(\overline{k},\overline{s}) = 1/\sqrt{2\pi}$ holds. From Eq. (28) the transformed Green's function follows as

$\bar{G}_{\mathrm{L}}(\bar{k},\bar{s}) = \bar{U}_{\mathrm{L}}(\bar{k},\bar{s}) = G_{\bar{U}\bar{U}}(\bar{k},\bar{s})/\sqrt{2\pi}$. Anyway, for the case when all kinds of damping are ignored $d_{\mathrm{ext}} = d_{\mathrm{int}} = \tau_r = 0$, an analytical solution may be derived. For the undamped bar, the transfer function of the displacement in the $(\bar{k}-\bar{s})$ - domain is, see Eq. (28)

$$\bar{G}_{\mathrm{L}}(\bar{k},\bar{s}) = \frac{1}{\sqrt{2\pi}} G_{\bar{U}\bar{U}}(\bar{k},\bar{s}) = \frac{1}{\sqrt{2\pi}} \frac{\bar{k}^2 + \tau_l \bar{s}^2}{\left(\tau_m \bar{s}^2 + \bar{k}^2\right)\left(\bar{k}^2 + \tau_l \bar{s}^2\right) + \alpha^2 \tau_l \bar{s}^2 \bar{k}^2}$$

$$= \frac{1}{\sqrt{2\pi}\left(w_1^2 - w_2^2\right)} \left[\frac{w_1^2 - \tau_l}{w_1^2 \bar{s}^2 + \bar{k}^2} + \frac{\tau_l - w_2^2}{w_2^2 \bar{s}^2 + \bar{k}^2} \right] \qquad (31)$$

with $\quad w_{1,2}^2 = \dfrac{\tau_m + \left(1+\alpha^2\right)\tau_l}{2} \pm \sqrt{\dfrac{\left(\tau_m + \left(1+\alpha^2\right)\tau_l\right)^2}{4} - \tau_m \tau_l}$.

Transformation into the Fourier domain $(\bar{k} - \bar{t})$ yields

$$\bar{U}(\bar{k},\bar{t}) = \frac{H(\bar{t})}{\sqrt{2\pi}\left(w_1^2 - w_2^2\right)} \left[\frac{w_1^2 - \tau_l}{w_1 \bar{k}} \sin(\bar{k}\bar{t}/w_1) + \frac{\tau_l - w_2^2}{w_2 \bar{k}} \sin(\bar{k}\bar{t}/w_2) \right], \qquad (32)$$

where the Heaviside function is denoted by the function $H(\bar{t})$.

Applying the inverse Fourier transformation, one finally obtains the Green's function for this problem

$$\bar{g}(\bar{x},\bar{t}) = \frac{H(\bar{t})}{2\left(w_1^2 - w_2^2\right)} \left\{ \frac{w_1^2 - \tau_l}{w_1} \left[H(\bar{x}+\bar{t}/w_1) - H(\bar{x}-\bar{t}/w_1) \right] \right.$$

$$\left. + \frac{\tau_l - w_2^2}{w_2} \left[H(\bar{x}+\bar{t}/w_2) - H(\bar{x}-\bar{t}/w_2) \right] \right\}. \qquad (33)$$

In extension to the wave equation of an elastic structure, there are two right-traveling wave fronts and two left-traveling wave fronts with different speeds $c_1 = 1/w_1$ (=slow traveling wave) and $c_2 = 1/w_2$ (=fast traveling wave), which occur in the arguments of the Heaviside functions $H(\bar{x} \pm \bar{t}/w_1)$ and $H(\bar{x} \pm \bar{t}/w_2)$.

If inductive electrodes (i.e., $\tau_l \to 0$ or $\tau_{l \ll \tau_{mech}}$) or piezoelectric coupling are negligible (i.e. $\alpha \to 0$), the two wave speeds are $c_1 \to \sqrt{1/\tau_{\mathrm{mech}}}$ and $c_2 \to \sqrt{1/\tau_l}$. From Eq. (33) the solution follows as

$$\tau_l \ll \tau_{mech} \text{ or } \alpha \to 0 : \bar{g}(\bar{x},\bar{t}) = \frac{H(\bar{t})}{2\sqrt{\tau_{mech}}} \left[H(\bar{x}+\bar{t}/\sqrt{\tau_{mech}}) - H(\bar{x}-\bar{t})/\sqrt{\tau_{mech}}) \right] \qquad (34)$$

which is the same as the solution for an elastic bar, see Graff (1991) pp. 25.

4.3 Numerical examples

In this section we study the wave-properties like wave-velocity, phase angle and wavenumber for various parameter combinations of a piezoelectric bimorph, see Fig. 3. First we only study conservative systems, i.e., mechanical damping or resistive electrodes are not considered (section 4.3.1). Then wave-characteristics are presented for dissipative systems, i.e., when mechanical damping $d_{\text{ext}} \neq 0, d_{\text{int}} \neq 0$ is accounted for or when the electrodes are assumed to be finitely conductive $\tau_r \neq 0$ (section 4.3.2). The parameters of the numerical example are listed in Table 1 (Appendix B). The characteristic length and the oscillation period for non-dimensionalization are chosen as $L = 0.5\,\text{m}$ and $\Omega = T^{-1} = 5698\,\text{s}^{-1}$. Since the mechanical wave speed is $c_{\text{mech}} = \sqrt{K_N / M_u} = 2849\,\text{ms}^{-1}$ (see Table 1 in Appendix B and Eq. (B.1) therein), the non-dimensional parameter is $\tau_m = 1$ and the non-dimensional coupling constant is $\alpha^2 = 0.089$, see Eq. (26). The other parameters $\tau_r, \tau_l, d_{\text{int}}$ and d_{ext} are considered as variables in our study.

4.3.1 Wave propagation of a non-damped piezoelectric bar

A first insight gives the frequency spectrum by solving the characteristic Eq. (29). Fig. 5 shows the excitation frequency $\bar{\omega}$ and the wave-speed $\bar{c} = \bar{\omega} / \bar{k}$ over the wave number $\bar{k}$. Ideal electrodes mean that the equipotential area condition of the voltage is satisfied ($\tau_r = \tau_l = 0$), i.e., the voltage does not depend on $\bar{x}$. The wave speed does not depend on the wave number $\bar{c} = 1$ (no dispersion). Considering no electrodes ($\tau_r \to \infty$), the differential Eq. (25) yields a linear relation between voltage and axial strain

$$\bar{v} = \frac{\alpha^2}{2} \bar{u}_{0,\bar{x}}. \tag{35}$$

Inserting this into Eq. (24), the non-dimensional longitudinal stiffness is increased by $(1 + \alpha^2)$

$$\tau_m \bar{u}_{0,\bar{t}\bar{t}} - \left(1 + \alpha^2\right) \bar{u}_{0,\bar{x}\bar{x}} = \bar{q}_{\bar{x}}, \tag{36}$$

yielding the characteristic equation $\tau_m \bar{s}^2 + \left(1 + \alpha^2\right) \bar{k}^2 = 0$ (see Eq. (29)). The result is a faster wave speed $\bar{c} = \tau_m / \left(1 + \alpha^2\right) = 1.04$ compared to ideal electrodes. Considering an electromechanically uncoupled configuration $\alpha = 0$ with inductive electrodes $\tau_l = 0.64$, two wave speeds exist: the mechanical wave traveling with $\bar{c}_{\text{mech}} = 1$, and the electrical one with $\bar{c}_{\text{elec}} = \sqrt{1 / \tau_l} = 1.25$. Taking into account the piezoelectric coupling, one finds the lower wave propagating with 0.93, the faster one with 1.33 (black-dotted line).

4.3.2 Wave propagation of a damped piezoelectric bar

The results for the dissipative piezoelectric bar are given in Fig. 6. Prescribing the frequency $\bar{\omega}$, the wave number $\bar{k}$ is complex-valued for these systems. The left figure shows the relation between $\bar{\omega}$ and $\mathrm{Re}\{\bar{k}\}$. Internal damping ($d_{\mathrm{int}} = 0.4$) means that the dissipation is related to the strain-rate: for low frequencies, the outcome is similar to the undamped beam, but for frequencies higher than $\bar{\omega} > 1$, damping needs to be accounted for. At $\bar{\omega} = 1$, the phase angle is $\varphi = 10.9°$ ($\tan\varphi = \mathrm{Im}\{\bar{k}\} / \mathrm{Re}\{\bar{k}\}$). Considering velocity dependent damping ($d_{\mathrm{ext}} = 0.4$), one recognizes from Fig. 6 (right) that damping is only relevant for very low frequencies. Including both kinds of mechanical damping ($d_{\mathrm{int}} = 0.4$, $d_{\mathrm{ext}} = 0.4$), the phase angle $\varphi = 21.8°$ is minimized at $\bar{\omega} = 1$, but it is $\varphi = 45°$ for $\bar{\omega} \to 0$ and $\bar{\omega} \to \infty$. The damping due to the resistive electrodes $\tau_r = 1$ has a maximum $\varphi = 1.27°$ at $\bar{\omega} = 1$: for very low and very high frequencies, electrical damping is not present. It is important to note that electrical damping cannot be reproduced by a linear combination of internal and external damping effects (see the phase angle for the limits $\bar{\omega} \to 0$ and $\bar{\omega} \to \infty$). In general, the case $\tau_r \neq 0$ yields two solutions for the wave-numbers, which are both complex-valued: roughly spoken, one solution is a slightly attenuated wave with a propagation speed of $\bar{c} \approx 1$, the second solution is an evanescent wave, i.e. a non-propagating wave. For electrodes with $\tau_r = 1$ and $\alpha \neq 0$, this phase angle is $\varphi \approx 45°$.
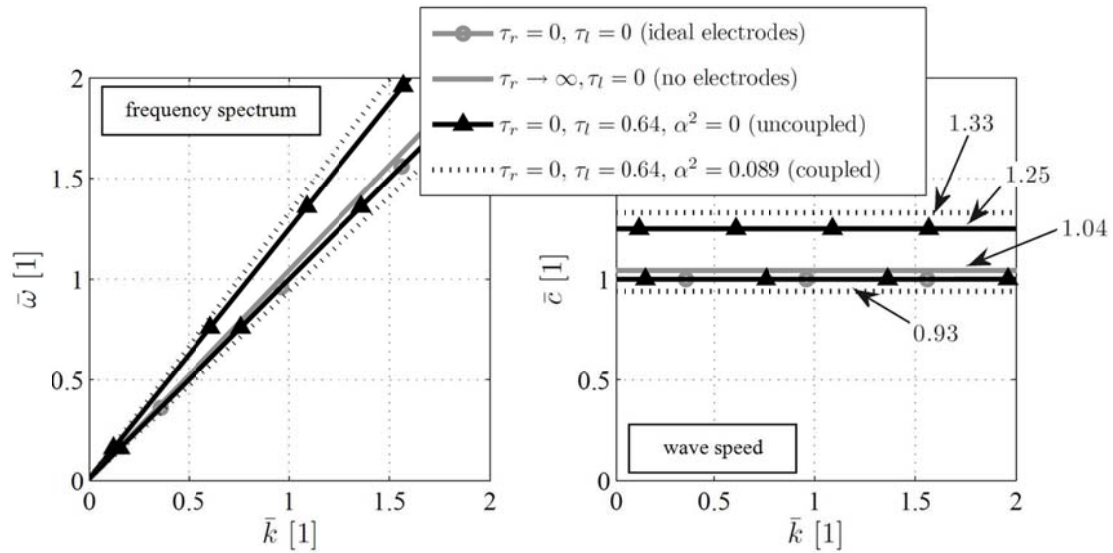

Fig. 5 Frequency spectrum $\bar{\omega}$ (left) and wave speed $\bar{c}$ (right) as functions of the wave-number $\bar{k}$ for a piezoelectric bar
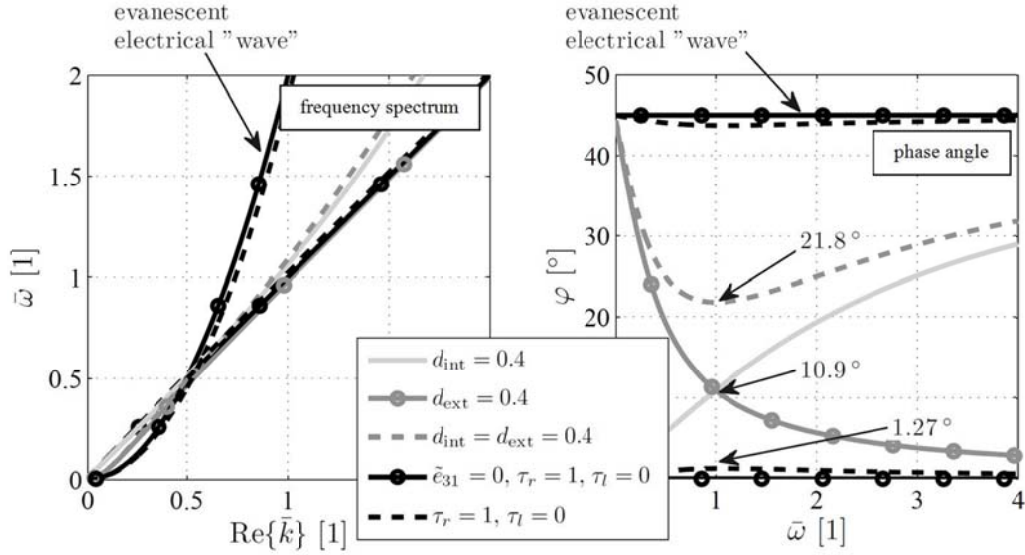
Fig. 6 Frequency spectrum $\bar{\omega}$ as a function of the wave-number $\mathrm{Re}\{\bar{k}\}$ (left) and phase angle φ as a function of the excitation frequency $\bar{\omega}$ (right) for mechanically and electrically damped bar

Fig. 7 shows the wave speed (top) and the phase angle (bottom) for various values of resistive-inductive electrodes (cases: $\tau_r \neq 0$, $\tau_l \neq 0$). For purely resistive electrodes ($\tau_r = 1$, $\tau_l = 0$ –black dashed) one sees the mechanical wave, which travels with $\bar{c} \approx 1$. Again, the second branch is the exponentially decaying, non-propagating (=the evanescent "electrical") wave. Taking into account resistive-inductive electrodes ($\tau_r = \tau_l = 1$ –light gray), one recognizes two wave fronts when increasing the excitation frequency ($\bar{c} = 0.87$ and $\bar{c} = 1.16$ for $\bar{\omega} \gg 1$). If the resistance is decreased, a similar behavior is obtained: for $\tau_r = 0.5$, $\tau_l = 1$ (gray-circle) the phase angle (of the lower branch) is maximized at $\bar{\omega} = 1$ and reads $\varphi \approx 3.71°$, whereas for $\tau_r = 0.1$, $\tau_l = 1$ (black-circle), the phase is a maximum at $\bar{\omega} = 0.2$. The phase angle diagram also shows that the hyperbola, which characterizes the $\varphi - \bar{\omega}$ curve of the second wave, is higher damped. These curves show that the damping performance of resistive-inductive electrodes is significantly much more efficient compared to the case of resistive electrodes, where the maximal phase angle is $\varphi_{\max} \approx 1.27°$. This is pointed out in the next section.

4.3.3 Harmonic response due to a single force

Next we investigate the response of the bar which is excited by the time-harmonic single force $\bar{q}_{\bar{x}}(\bar{x}, \bar{t}) = \delta(\bar{x})\cos(\bar{t})$, i.e. at the frequency $\bar{\omega} = 1$. Consequently, the response of the bar will be also time-harmonic, and depending on the dissipative properties of the system, the disturbance will spatially decay. We are mainly interested in the damping capabilities of the electrodes to show that this technology might be useful for technical applications.
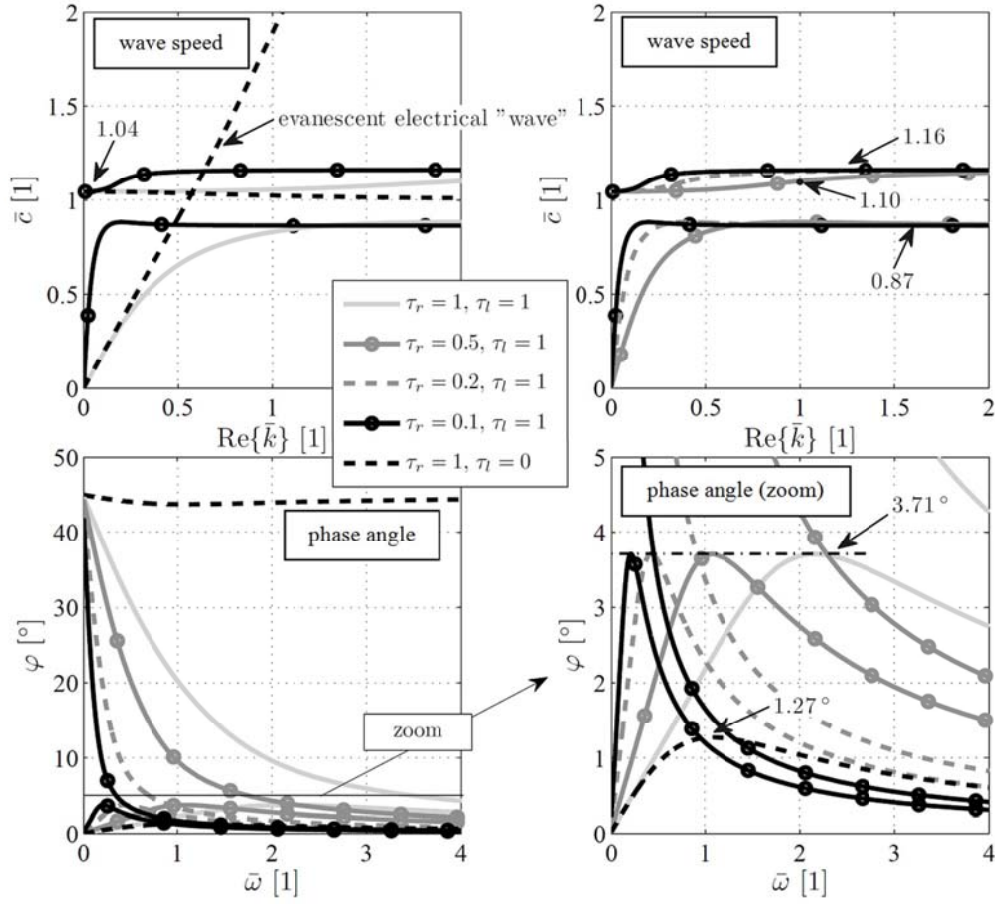
Fig. 7 Wave speed $\bar{c}$ as a function of the wave-number $\mathrm{Re}\{\bar{k}\}$ (above) and phase angle φ over the excitation frequency $\bar{\omega}$ (bottom) for bar with resistive and/or inductive electrodes

As already known from Figs. 6 and 7, the phase angle for the resistive electrodes $\tau_r = 1$ is maximal for $\bar{\omega} = 1$ ($\varphi_{\max} = 1.27°$). But, also for the case $\tau_r = 0.5$ and $\tau_l = 1$, the phase is optimized at $\bar{\omega} = 1$ ($\varphi_{\max} = 3.71°$). Anyway, from the frequency spectra curves it is difficult to conclude what this means for harmonic excitations, e.g. from a practical point of view it is interesting to know at which distance the disturbances are almost attenuated. In Fig. 8, bars with resistive and resistive-inductive electrodes are compared to mechanically damped bars (case 1: $d_{\mathrm{ext}} = 0.05, d_{\mathrm{int}} = 0$ (light-gray), case 2: $d_{\mathrm{ext}} = 0, d_{\mathrm{int}} = 0.03$ (gray)). The steady-state responses as a function of the axial coordinate are drawn for various time steps $\bar{t}_1 = 0, \bar{t}_2 = 0.4\pi$ and $\bar{t}_3 = 0.8\pi$.
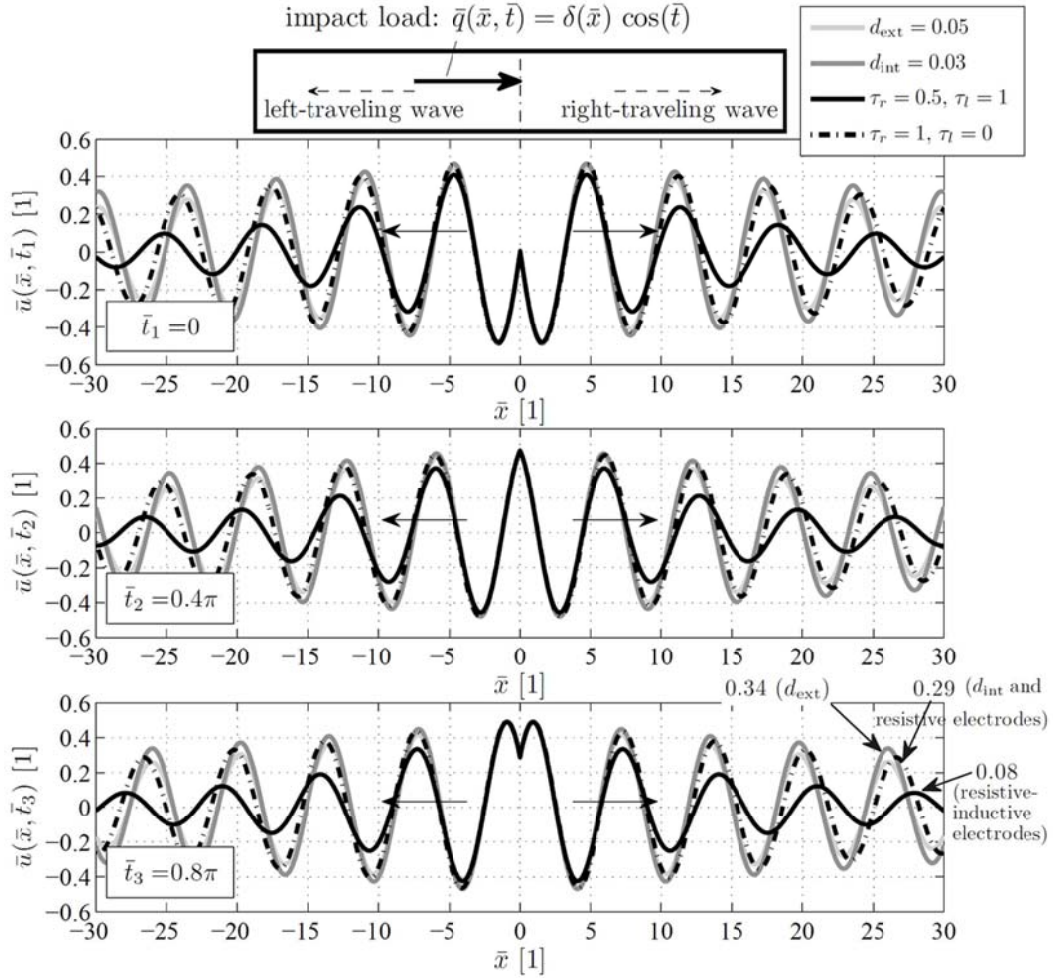
Fig. 8 Longitudinal wave propagation due to a harmonic impact load $\delta(\overline{x})\cos(\overline{t})$ for a mechanically damped piezoelectric bar with perfect electrodes ($d_{\text{ext}} = 0.05, d_{\text{int}} = 0.03$), for a mechanically undamped bar with resistive-inductive ($\tau_r = 0.5, \tau_l = 1$) and with resistive electrode properties ($\tau_r = 1, \tau_l = 0$). Three consecutive instants of time $\overline{t_1}$, $\overline{t_2}$ and $\overline{t_3}$ are shown

One observes that the wave speed is $\overline{c} \approx 1$ for the internally ($d_{\text{int}} = 0.03$ –gray) and the externally damped bar ($d_{\text{ext}} = 0.05$ –light gray) and for the bar with resistive electrodes ($\tau_r = 1, \tau_l = 0$ –dashed-black). For the resistive-inductive ($\tau_r = 0.5, \tau_l = 1$ – black), the wave speed is slightly faster $\overline{c} \approx 1.10$. At $\overline{x} \approx 27$ the amplitude of the wave for the internally damped bar is 0.34 (reduction of -32% compared to the deflection amplitude at the origin $\overline{x} = 0$, which is 0.5), which is higher than the resistively damped harmonic wave 0.29 (-42%) at the same location. The outcome of the electrical damping ($\tau_r = 1, \tau_l = 0$) is close to the results, when the

external damping of the bar is $d_{\text{ext}} = 0.05$. In comparison to this, the amplitude for the resistive-inductive electrodes is much lower, it is only 0.08 (reduction -84%). This is less than one sixth of the displacement at the origin $\bar{x} = 0$. From a practical point of view, the vibrations are almost completely damped out at $\bar{x} \approx 27$, which is 4 times of the wavelength, and thus showing the huge potential of resistive and inductive electrodes, in particular for passive vibration control.

5. Conclusions

In the present contribution, a new one-dimensional theory for smart piezoelectric beams is derived, which considers non-ideal electrodes. Here, we assume the electrodes to have resistive and inductive properties for our approach. The outcome is an extended beam theory with coupled differential equations for the longitudinal and the lateral beam deflections and an additional differential equation (Telegrapher's equation) for the calculation of the voltage distribution along the beam axis. Furthermore, for the special case of an infinitely long, piezoelectric longitudinal bar equipped with non-ideal (resistive-inductive) electrodes, the non-dimensional equations of motions are presented. The frequency spectra are calculated (wave-numbers, wave speeds and phase angles) and the results for a time-harmonic excitation load is presented. For purely inductive electrodes it is shown that the traveling wave fronts propagate with two different wave speeds. It is found that purely resistive and resistive-inductive electrodes may be considered as candidates to attenuate structural vibrations. In case of resistive-inductive electrodes it is shown that an optimal choice of the electrical properties may efficiently attenuate the axial displacement of a bar.

Acknowledgments

References

Abramovich, M. and Stegun, I. (1972), *Handbook of Mathematical Functions with Formulas, Graphs, and Mathematical Tables*, Dover, New York.

Buchberger, G., Barb, R.A., Schoeftner, J., Bauer, S., Hilber, W., Mayrhofer, B. and Jakoby, B. (2015), "Transparent, flexible and thin sensor surfaces for passive light-point localization based on two functional polymers", *Sensor. Actuat. A - Phys.*, **239**, 70-78.

Buchberger, G. and Schoeftner, J. (2013), "Modeling of slender laminated piezoelastic beams with resistive electrodes – comparison of analytical results with three-dimensional finite element calculations", *Smart Mater. Struct.*, **22**, 032001 (13pp).

Buchberger, G., Schwoediauer, R., Arnold, N. and Bauer, S. (2008b), "Cellular ferroelectrets for flexible touchpads, keyboards and tactile sensors", *IEEE Sensors Conference Proceedings* 2008, **10**, 1520-1523.

Buchberger, G., Schwoediauer, R. and Bauer, S. (2008), "Flexible large area ferroelectret sensors for location sensitive touchpads", *Appl. Phys. Lett.*, **92**, 123511 (3 pages).

Crawley, E.F. (1994), "Intelligent structures for aerospace: a technology overview and assessment", *AIAA J.*, **32**(8), 1689-1699.

Ding, L., Zhu, H.P. and Yin, T. (2013), "Wave propagation in a periodic elastic-piezoelectric axial-bending coupled beam", *J. Sound Vib.*, **332**(24), 6377-6388.

Forward, R.L. (1979), "Electronic damping of vibrations in optical structures", *Appl. Opt.*, **18**(5), 670-677.

Graff, K.F. (1991), *Wave motion in elastic solids*, Dover, New York.

Jansson, A. and Lundberg, B. (2007), "Piezoelectric generation of extensional waves in a viscoelastic bar by use of a linear power amplifier: Theoretical basis", *J. Sound Vib.*, **306**(1-2), 318-332.

Jansson, A. and Lundberg, B. (2008), "Three-port impedance model of a piezoelectric bar element: Application to generation and damping of extensional waves", *J. Sound Vib.*, **315**(4-5), 985-1012.

Kolsky, H. (1963), *Stress waves in solids*, Dover, New York.

Krawczuk, M., Grabowska, J. and Palacz, M. (2006), "Longitudinal wave propagation. Part I-Comparison of rod theories", *J. Sound Vib.*, **295**(3-5), 461-478.

Krommer, M. (2001), "On the correction of the Bernoulli-Euler beam theory for smart piezoelectric beams", *Smart Mater. Struct.*, **10**(4), 668-680.

Lediaev, L. (2010), "Finite element modeling of piezoelectric bimorphs with conductive polymer electrodes", doctoral thesis Montana State University, Bozeman, Montana.

Lin, X. and Yuan, F.G. (2001), "Diagnostic Lamb waves in an integrated piezoelectric sensor/actuator plate: analytical and experimental studies", *Smart Mater. Struct.*, **10**(5), 907-913.

Miu, D.K. (1993), *Mechatronics: Electromechanics and Contromechanics*, New York, Springer.

Rose, J.L. (2004), *Ultrasonic waves in solid media*, Cambridge, Cambridge University ².

Schoeftner, J. and Buchberger, G. (2013), "Verfahren zur Aenderung des statischen und/oder dynamischen Istverhaltens eines insbesondere elastischen Koerpers unter aeusserer Belastung", Patent 513259, filed January 29th, 2013 and issued March 15th, 2014.

Schoeftner, J., Buchberger, G. and Benjeddou, A. (2015b), "Transverse dynamics of slender piezoelectric bimorphs with resistive-inductive electrodes" (submitted simultaneously for publication in *Smart Struct. Syst.* 2016)

Schoeftner, J., Buchberger, G., Brandl, A. and Irschik, H. (2015), "Theoretical prediction and experimental verification of shape control of beams with piezoelectric patches and resistive circuits", *Compos. Struct.*, **133**, 746-755.

Schoeftner, J., Buchberger, G. and Irschik, H. (2014), "Static and dynamic shape control of slender beams by piezoelectric actuation and resistive electrodes", *Compos. Struct.*, **111**, 66-74.

Tzou, H.S. (1998), "Multifield transducers, devices, mechatronic systems and structronic systems with smart materials", *Shock Vib. Dig.*, **30**(4), 282-294.

Vivar-Perez, J.M., Duczek, S. and Gabbert, U. (2014), "Analytical and higher order finite element hybrid approach for an efficient simulation of ultrasonic guided waves I: 2D-analysis", *Smart Struct. Syst.*, **13**(4), 587-614.

Yuan, W.C., Zhou, L. and Yuan, F.G. (2008), "Wave reflection and transmission in composite beams containing semi-infinite delamination", *J. Sound Vib.*, **313**(3-5), 676-695.

FC

Appendix A

The general beam Eqs. (11) and (12), where the electrode properties and the longitudinal and lateral deformations are considered, require the knowledge of the axial, the coupling and the bending stiffness $K_{\mathrm{N}}, K_{\mathrm{NM}}$ and K_{M} and the mass per unit length $M_w = M_u$ terms. They read for a beam with k layers

$$
\begin{aligned}
K_{\mathrm{N}} &= \sum_k \tilde{C}_{11}^k \left(z_{2k} - z_{1k} \right) b_k \\[4pt]
K_{\mathrm{NM}} &= \sum_k \tilde{C}_{11}^k \frac{z_{2k}^2 - z_{1k}^2}{2} b_k \\[4pt]
K_{\mathrm{M}} &= \sum_k \tilde{C}_{11}^k \frac{z_{2k}^3 - z_{1k}^3}{3} b_k + \frac{\left(\tilde{e}_{31}^k \right)^2}{\tilde{\kappa}_{33}^k} \frac{\left(z_{2k} - z_{1k} \right)^3}{12} b_k \\[4pt]
M_w &= M_u = \sum_k \rho_k \left(z_{2k} - z_{1k} \right) b_k .
\end{aligned}
\tag{A.1}
$$

Appendix B

The parameters for the bimorph bar (used in the numerical examples presented in section 4.3) are listed in Table 1.

Table 1 Parameters for the numerical examples

variable (unit)	value
$\rho_{\mathrm{p}}\ (\mathrm{kg/m^3})$	7750
$z_{1\mathrm{p}}\ (\mathrm{m})$	0
$z_{2\mathrm{p}}\ (\mathrm{m})$	$5.00 \cdot 10^{-4}$
$b_{\mathrm{p}}\ (\mathrm{m})$	$5.00 \cdot 10^{-2}$
$\tilde{e}_{31}^{\mathrm{p}}\ (\mathrm{As/m^2})$	-10.94
$\tilde{\kappa}_{33}^{\mathrm{p}}\ (\mathrm{As/V/m})$	$2.15 \cdot 10^{-8}$
$\tilde{C}_{11}^{\mathrm{p}}\ (\mathrm{Nm^2})$	$6.29 \cdot 10^{10}$

The layer thickness h_p, the mean distance to the x-axis $z_{\mathrm{m}p}$, the mass per unit length M_u, the longitudinal stiffness K_{N}, the capacity per unit length c read (see also A.1)

$$h_p = z_{2p} - z_{1p} = 5.00 \ 10^{-4} \ \text{m}$$

$$z_{mp} = \frac{z_{2p} + z_{1p}}{2} = 2.50 \ 10^{-4} \ \text{m}$$

$$M_u = 2\rho_p b_p h_p = 0.3875 \ \text{kg/m} \qquad\qquad \text{(B.1)}$$

$$K_N = 2\widetilde{C}_{11}^p b_p h_p = 3.15 \ 10^6 \ \text{N}$$

$$c = \widetilde{k}_{33}^p b_p / h_p = 2.15 \ 10^{-6} \ \text{As/V/m}$$